Journal Name

ARTICLE TYPE

Theoretical Analysis of Crystallization by Homogeneous Nucleation of Water Droplets

Kyoko K. Tanaka,*[a] and Yuki Kimura[b]

We propose a novel method of analyzing the crystallization process from supercooled water droplets. The method, which is based on nucleation theory, simultaneously evolves the homogeneous ice nucleation, and crystal growth in the cooling process and obtains the crystallization temperature and the number of crystal nuclei in the droplet. The model can reproduce not only the crystallization of water but also vitrification process. The model well replicated the results of previous laboratory experiments, especially, the different responses of the crystallization temperatures of the micrometer- and nanometer-sized particles as functions of cooling rate. For particle sizes ranging from 1 to 1000 μm and cooling rates below 10^4 Ks^{-1}, the crystallization temperature was 230-240 K. At cooling rates above 10^4 Ks^{-1}, the crystallization temperature decreased rapidly. On the other hand, the crystallization temperature of 10 nm particles was 200–230 K at cooling rates below 10^4 Ks^{-1}. When describing the interfacial tension by $\sigma = 29.1 + 0.1(T - 273.15)$ erg cm^{-2} (where T is the water droplet temperature in K), the analyses explained well the previously reported crystallization temperatures of droplets sized from a few nm to 100 μm under various cooling conditions. Our model also predicts the critical cooling rate for vitrification of the liquid water droplets. The critical cooling rate of vitrification is predicted as $10^7 - 10^8$ Ks^{-1}, consistent with the experimental rates. These analyses are useful not only for comprehensively understanding the ice nucleation process but also for predicting the crystallization processes in various environments such as cirrus clouds, which are difficult to reproduce in experiments.

1 Introduction

The crystallization process of water droplets is of great practical and fundamental importance in science and technology and is largely dependent on climate. For instance, supercooled water droplets are often observed at very low temperatures ($\simeq$ 235 K), below the equilibrium melting temperature in the Earth's troposphere[1]. The temperature of homogeneous nucleation (235 K) is often called the homogeneous ice nucleation limit (or temperature), but this is a practical definition only because the actual temperature of homogeneous nucleation depends on the droplet size, cooling rate, and other conditions[2]. Understanding of the ice nucleation kinetics is important for determining the efficiency of ice particle formation in clouds.

Homogeneous ice nucleation of water droplets has been explored in numerous experiments using a variety of methods such as expansion cloud chambers, the supersonic nozzle method, optical microscopy, and levitation[3–13]. Table 1 lists the crystallization temperatures of pure water droplets at various cooling rates (on the order of 10^{-3} to 10^5 Ks^{-1}) and droplet sizes (from a few nm to 100 μm). The crystallization temperature ranges from 200 to 240 K. However, when the cooling rate is extremely large, the water droplets vitrify rather than crystallize. In several experiments, pure liquid water has been vitrified by high pressure jet freezing. The critical cooling rate that vitrifies liquid water was suggested to exceed $10^6 - 10^7$ Ks^{-1}, but the exact cooling rate is not clarified yet.

Figure 1 plots the crystallization temperatures and vitrification conditions as functions of cooling rate. The characteristics of these plots are summarized below.

- The crystallization temperature of micrometer-sized droplets is around 235 K over a wide range of cooling rates (from 10^{-3} to 10^4 Ks^{-1}). Moreover, different methods yield similar values[3,5–10,12].
- For small (nm-sized) droplets, the crystallization temperature drops into the "no man's land" region ($\sim$ 200 K) at high cooling rates ($\simeq 10^5$ Ks^{-1})[4,11].
- The liquid water droplets vitrify at cooling rates above $10^6 - 10^7$ Ks^{-1}[2,14,15].

In the previous studies, various parameterizations of the rate of homogeneous ice nucleation were performed based on classical nucleation theory[12,13,16,17]. The key terms in classical theory

[a] Tohoku University, 985-8578, Sendai, Japan. Tel: +81-22-795-6501; E-mail: kk-tanaka@astr.tohoku.ac.jp
[b] Institute of Low Temperature Science, Hokkaido University, 060-0819, Sapporo, Japan.

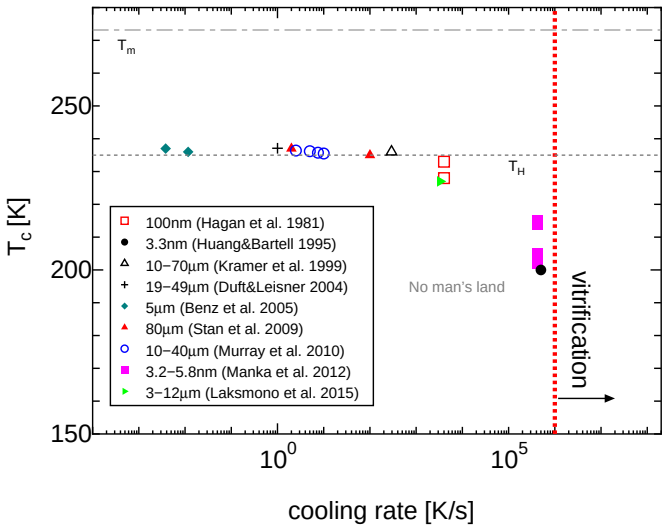

Fig. 1 Crystallization temperature versus cooling rate in various experiments of homogeneous ice nucleation of water droplets shown in Table 1. $T_{\rm H}(=235$ K) is called the homogeneous nucleation temperature. The water droplets vitrify at extremely large cooling rates $\gtrsim 10^6-10^7$ Ks^{-1}.

are the self-diffusion energy and the ice-liquid interfacial energy between the ice embryo and supercooled water[13,16]. These values are determined by fitting the classical model to laboratory homogeneous ice nucleation data sets. On the other hand, in the laboratory experiments, the crystallization temperatures are measured and the nucleation rate was evaluated from the obtained crystallization temperature under two assumptions: fixed temperature of water droplets (isothermal condition) and a single nucleus in the water droplet. The number of nuclei generally depends on the laboratory condition, thus the single nucleation is not valid for cases of rapid cooling rate and large droplet size.

By comprehensively understanding the results of diverse experiments, we could not only elucidate the ice nucleation process of droplets but could also predict the crystallization process in various environments, which is difficult to achieve in experiments. However, the characteristics of the above mentioned experimental results have never been explained by an all-encompassing analysis. Motivated by this deficit, we construct a new model of water-droplet crystallization that evolves the processes of homogeneous nucleation and crystal growth during cooling.

In the previous models, different experiments were compared in terms of the nucleation rates, but would be more directly compared in terms of their crystallization temperatures because the method of evaluating the nucleation rate differs among experiments. In this study, we can obtain the crystallization temperature and compare directly the experimental data. Furthermore, we obtain the evolution of number of nuclei in a droplet. The model reproduces not only the crystallization of water but also vitrification process. The model explains well most of the experimentally obtained crystallization temperatures of supercooled water droplets and evaluates the crystallization temperatures in various environments. Our analysis can also predict the critical cooling rate of vitrification. The analytical model of the crystallization process assists our understanding of ice nucleation and predict the crystallization process in environments that cannot be replicated in the laboratory. Section 2 of this paper describes the model of crystallization of water droplets, which solves the time evolutions of homogeneous ice nucleation and crystal growth throughout the cooling process. The model obtains the crystallization temperature and the number of crystal nuclei. Section 3 presents the results and compares them with the results of previous experiments. The study is summarized in Section 4.

2 Basic equations

In general, droplets crystallize by two consecutive processes: the nucleation from liquid to crystal and crystal growth of the nuclei. These processes rely on two important quantities. First is the surface energy at the liquid-solid interface, which determines the nucleation rate from liquid to crystal. The other is the activation energy of molecular diffusion in the liquid[16]. We consider the crystallization of liquid droplets while cooling from the melting temperature $T_{\rm m}(=273.15$ K). This study revises our previous model[18], which determines the interfacial tension σ between melt and the crystalline phase, and the activation energy $E_{\rm a}$ of molecular diffusion in a silicate melt. The model in[18] ignores the size dependence of the crystallization process because it assumes a fixed droplet size and many nuclei in the droplet. In fact, if the number of nuclei in the droplet is much larger than unity, the size effect vanishes because there is no size dependence in the temperature-dependent nucleation and growth rates. However, the crystallization process of smaller droplets starts later than that of larger droplets because growth requires at least one nucleus. The present study incorporates the size effect.

The nucleation rate is calculated as[2]:

$$J = nZf \exp\left\{-\frac{\Delta G^*}{kT}\right\}, \tag{1}$$

where n is the number density of the molecules in the liquid particle, T is the droplet temperature, k is the Boltzmann constant, f is the attachment rate of molecules to a critical nucleus with size i_*, and Z is a factor called the Zeldovich factor. Using the impinging rate of molecules per surface molecule $Dn^{2/3}$ (where D is the self-diffusion coefficient) and the number of surface molecule of a critical nucleus $Ai_*^{2/3}n^{2/3}$, f is given by

$$f = Ai_*^{2/3}n^{4/3}D, \tag{2}$$

with

$$D = D_0 \exp\left(-\frac{E}{kT}\right), \tag{3}$$

where E is the activation energy of diffusion and D_0 is a constant. ΔG^* in Eq.(1) is the minimum work of forming an embryo of critical size i_*. ΔG is given by

$$\Delta G = -\Delta\mu i + \sigma A i^{2/3}, \tag{4}$$

Table 1 Sizes, cooling rates, and crystallization temperatures T_c [K] of water droplets obtained in various experiments

size	cooling rate [Ks^{-1}]	T_c [K]	method	reference
3.3 nm	5.0 $\times 10^5$	200	Supersonic nozzle	[4]
3.2 nm	(4-4.5) $\times 10^5$	202	Supersonic nozzle	[11]
3.5 nm	(4-4.5) $\times 10^5$	205	Supersonic nozzle	[11]
4.3 nm	(4-4.5) $\times 10^5$	214	Supersonic nozzle	[11]
5.8 nm	(4-4.5) $\times 10^5$	215	Supersonic nozzle	[11]
0.1μm	4.0 $\times 10^3$	228	Expansion cloud chamber	[3]
7.5 μm	3.3 $\times 10^3$	227	Gas dynamic virtual nozzle	[12]
0.1 μm	4.0 $\times 10^3$	233	Expansion cloud chamber	[3]
20 μm	10	235.5	Cold stage	[10]
20 μm	7.5	235.75	Cold stage	[10]
20 μm	5	236.2	Cold stage	[10]
20 μm	2.5	236.4	Cold stage	[10]
80 μm	2-100	235-237	Microfluidic instrument	[9]
5 μm	(0.38-1.166) $\times 10^{-2}$	236-237	Large aerosol chamber	[7]
(140-490) μm	0.1 -1.3	237.1	Levitator	[6]
(10-70) μm	293	236-237	Levitator	[5]

where σ is the interfacial tension between the liquid and crystalline material and $Ai^{2/3}$ is the surface area of a size-i embryo. For a sphere, $A = 4\pi r_0^2 i^{2/3}$ with r_0 (the mean inter-particle separation in the liquid phase). $\Delta\mu$ is the difference of the chemical potential between liquid and crystalline phases. It is calculated as $\Delta\mu = kT\ln(P_{sw}/P_{si})$, where P_{sw} and P_{si} are the saturation vapor pressures over liquid water and ice, respectively. At the critical size $i_* = [2A\sigma/(3\Delta\mu)]^3$ and given $Z = \sqrt{A\sigma/(\pi kT)}/(3i_*^{2/3})$, the nucleation rate is rewritten as[2,19,20]

$$\begin{aligned} J &= \frac{A}{3}n^{7/3}\sqrt{\frac{A\sigma}{\pi kT}}D \\ &\quad \times \exp\left\{-\frac{4}{27}\frac{[A\sigma/(kT)]^3}{[\ln(P_{sw}/P_{si})]^2}\right\}. \end{aligned} \tag{5}$$

Meanwhile, the growth rate of crystalline phase is given by[21,22]

$$\frac{da}{dt} = Dn^{1/3}\left[1-\exp\left(-\frac{\Delta\mu}{kT}\right)\right], \tag{6}$$

where a is the crystal radius. The second term in the bracket in Eq.(6) describes the effect of the latent heat deposition, which re-melts crystalline surface.

We consider a cooling gas with a cooling rate $u(= dT_{gas}/dt)$ and melt droplet cooling by heat conduction through the ambient gas and thermal radiative cooling. The gas temperature T_{gas} and droplet temperature T are, respectively, given by

$$\begin{aligned} T_{gas} &= T_m - ut, \\ \frac{4}{3}\pi r^3\rho_d C_d\frac{dT}{dt} &= -4\pi r^2\alpha(T-T_{gas}) \\ &\quad -4\pi r^2\sigma_{SB}\varepsilon(T^4-T_{gas}^4)+H, \end{aligned} \tag{7}$$

where the droplet is assumed isothermal because of its small size. C_d is molar heat capacity and ρ_d is the density of the droplet[18]. The first term on the right-hand side of Eq.(7) describes conductive cooling. α is the heat transfer coefficient of the ambient gas, which generally depends on the gaseous number density n_g, i.e., $\alpha \simeq 2n_g v_{th}k$, v_{th} is the thermal velocity of gas[18]. In this study, α is determined by fitting the given cooling rate. The second term on the right-hand side of Eq.(7) is thermal radiative cooling, and σ_{SB} and ε are the Stefan Boltzmann constant and efficiency of thermal radiation emission, respectively. H is the heating rate due to deposited latent heat of crystallization, expressed by

$$H = \frac{4}{3}\pi a^3\rho_d L\frac{d\theta}{dt}, \tag{8}$$

where L is the latent heat of crystallization per unit mass.

The number $N(t')$ of critical crystal nuclei in a particle formed between times t' and $t'+dt'$ is

$$N_v(t')dt' = [V_0 - V_c(t')]J(t')dt', \tag{9}$$

where the nucleation rate J is the number of nuclei formed per unit time per unit volume, V_0 is the volume of initial liquid particle, and V_c is the crystal volume in the particle, given by

$$V_c(t) = \int_0^t [V_0 - V_c(t')]J(t')\beta_v a^3(t,t')dt', \tag{10}$$

where $\beta_v a^3$ is the volume of a growing crystalline nucleus. The geometrical factors β_v depends on the morphology of the crystal growth; for spherical growth (as assumed in this study), $\beta_v = 4\pi/3$. Using (10) and the volume fraction of the crystal in the particle, $\theta \equiv V_c/V_0$ is given by

$$\theta(t) = \begin{cases} 0 & t < t_0, \\ \int_0^t [1-\theta(t')]J(t')\beta_v a^3(t,t')dt' & t_0 < t, \end{cases} \tag{11}$$

where t_0 is the onset time of ice nucleation with unity number of critical nuclei N_v in a particle. It should be noted that the condition (11), which involves t_0, is excluded in[18]. From Eq.(9), N_v is given by

$$N_v(t) = \int_0^t N(t')dt' = \int_0^t [V_0 - V_c(t')]J(t')dt'. \tag{12}$$

Solving Eqs. (5), (6), (7), and (11), we obtain the time evolutions of nucleation rate,crystal growth, particle temperature, and volume fraction of the crystal, respectively. In solving these equations, we need several thermal quantities of water. Especially im-

portant quantities are the liquid-solid interfacial surface tension and the activation energy of diffusion of molecules in liquid. Fortunately, many data of interfacial tension for water are available within some range. In this study, we adopt the liquid-solid interfacial tension given by

$$\sigma = 29.1 + 0.1(T - 273.15) \text{erg cm}^{-2}, \quad (13)$$

where the interfacial tension at the melting point $\sigma_0 = 29.1$ erg cm^{-2} was evaluated in [23] and was recommended in late studies [16,24]. As the crystallization temperature depends largely on the interfacial tension, we varied the interfacial tension in the model calculations. According to our results, the interfacial tension given by Eq.(13) can explain most of the water crystallization results obtained in previous experiments, as will be shown in Section 3.

We adopt two sets of diffusivity data. The first is diffusivity for amorphous ice (ASW), determined by [26]:

$$D = 2.8 \times 10^{-3} \exp\left(\frac{-892}{T - 119}\right) \text{cm}^2\text{s}^{-1}. \quad (14)$$

The second is the diffusivity of supercooled liquid (SCL) water [27], which is extrapolated to low temperature with Arrhenius equation:

$$D = 1.5 \times 10^{-2} \exp\left(\frac{-2045}{T}\right) \text{cm}^2\text{s}^{-1}. \quad (15)$$

Fig. 2 plots the diffusivities of ASW and SCL versus temperature. There is no large difference between two diffusivities at temperatures above 230 K, but at lower temperatures, the SCL diffusivity is much lower than the ASW diffusivity. It should be noted that Eq. (15) agrees well with the diffusivity at $T \simeq 60$ K obtained by [28], who demonstrated that liquid-like water forms from the UV-irradiated vapor-deposited amorphous ice around 50-140 K. The other thermal quantities of water adopted in this study are shown in Table 2.

As the previous studies suggested, the internal pressure in nanometer-droplets is several orders greater than in a micrometer-droplet due to the Laplace pressure [12,13]. The large pressure may cause the deviation of the self-diffusion coefficient D in nanometer-sized water droplets, but the effect would not be large because the pressure dependence of D in liquid is generally small. However, there is another possibility that the self-diffusion in nanometer-droplets is larger than the bulk value because of the surface effect, i.e., the molecules in small droplets were more diffusive than in the bulk liquid due to the surface effect of the finite boundary [31]. This effect increases the nucleation rate, although the dependency is not fully understood yet. Furthermore, it is suggested that the interfacial tension between liquid water and ice in nanometer-droplets deviates from bulk value due to the pressure effect [17]. If the interfacial tension in nanometer droplets is larger than the bulk value, the nucleation rate decreases [17]. Because of the lack of thermodynamic quantities in nanometer droplets, we did not take into account the size dependence. Additional future experiments for nanometer-sized droplets will provide constraints for thermodynamic quantities and improve the analysis for small droplets.

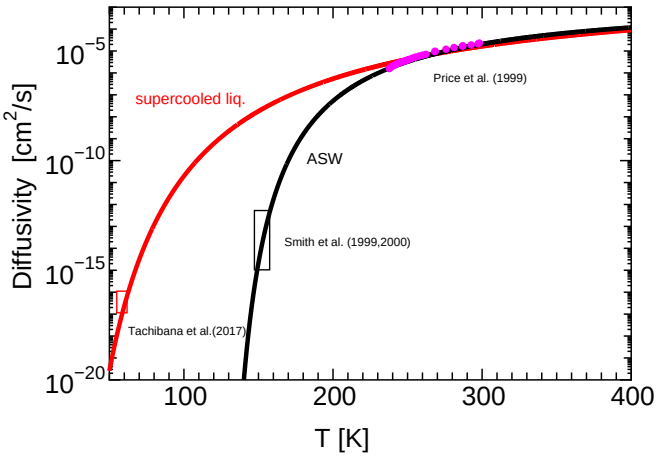

Fig. 2 Diffusion coefficients of amorphous ice (ASW, black) given by Eq.(14) [25,26] and supercooled liquid water (SCL, red) given by Eq.(15) [27] as functions of temperature. The diffusivity at $T = 60$ K obtained by [28] with the use of $D = kT/(6\pi\eta r_o)$ with viscosity η, is also shown.

3 Results and discussion

Figure 3 shows a typical example of the model simulations. The droplet is 10 μm in size, and the cooling rate is 30 Ks^{-1} with $\alpha = 1.1 \times 10^5$ erg s^{-1}cm^{-2}K^{-1} and $\varepsilon = 1$. Fig. 3(a) shows the evolving temperature of the water droplet. The droplet starts to crystallize at $T = 235$ K at $t = 1.4$ s. Hereafter, the temperature at which crystallization begins is called the crystallization temperature T_c. The temperature jumps from the crystallization temperature to the melting point T_m as latent heat of crystallization is released. Fig.3(b) shows the number of critical nuclei included in a droplet (left vertical axis) and the volume ratio of the crystal to initial volume (right vertical axis) over time.

In this case, the number of critical nuclei is unity, and the number of molecules included in a critical nucleus is 111. The crystallization proceeds because of the growth of the critical nucleus. The nucleation rate increases as the temperature decrease over time (Fig.3(c)), but nucleation ceases after the start of crystallization because the temperature rapidly increases at that time.

Figure 4 shows the same evolutions as Fig. 3 but for various cooling rates. The crystallization temperature is very similar at the three cooling rates, showing a slight increase as the cooling rate reduces: $T_c = 234$, 235, and 236 K at the cooling rates of 30, 3.0, and 0.3 Ks^{-1}, respectively. The number of critical nuclei is unity in all cases, indicating that the crystallization proceeds quickly once the nucleus forms and the single crystal forms. The numbers of molecules in the critical nucleus are 111, 115, and 120 at cooling rates of 30, 3.0, and 0.3 Ks^{-1}, respectively. As

Table 2 Physical properties of water

property	value	reference
molecular weight M_{H2O} [g mol^{-1}]	18.015	29
density of liquid ρ_d	$0.08\tanh((T-225)/46.2)+0.7415((647.15-T)/647.15)^{0.33}+0.32$	29
Equilibrium vapor pressure [Pa]		
liquid P_{sw}	$\exp(54.842763-6763.22/T-4.210\ln(T)$ $+0.000367T+\tanh(0.0415(T-218.8))\times$ $(53.878-1331.22/T-9.44523\ln(T)+0.014025T))$, $123<T<332$ K	30
ice P_{si}	$\exp(9.550426-5723.265/T+3.53068\ln(T)$ $-0.00728332T)$ at $T>110$ K	30
molar heat capacity C_d [Jmol^{-1}K^{-1}]	$-2.0572+0.14644T+0.06163T\exp\{-(T/125.1)^2\}$, $T>20$ K	30

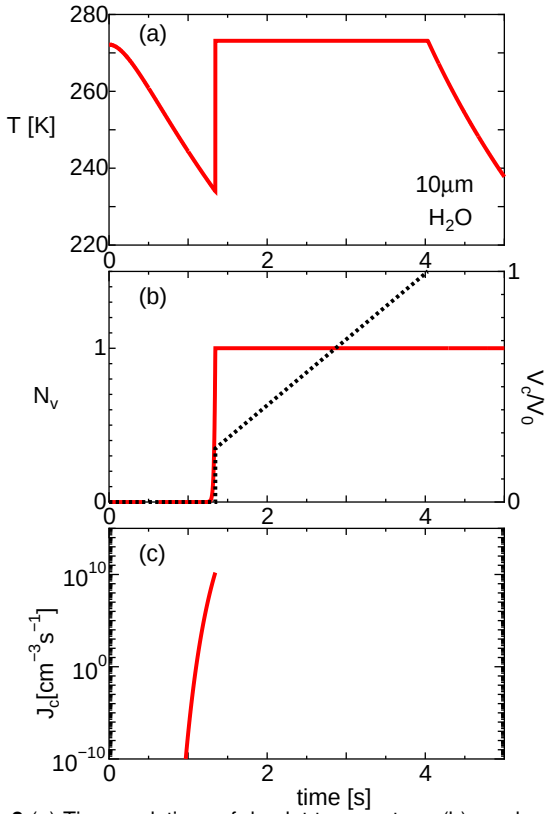

Fig. 3 (a) Time evolutions of droplet temperature, (b) number of critical nuclei in the droplet (left vertical axis, red solid line) and volume ratio between the crystal and initial volumes (right vertical axis, black dotted line), and (c) nucleation rate. The droplet is 10 μm in size, and the cooling rate is 30 Ks^{-1}.

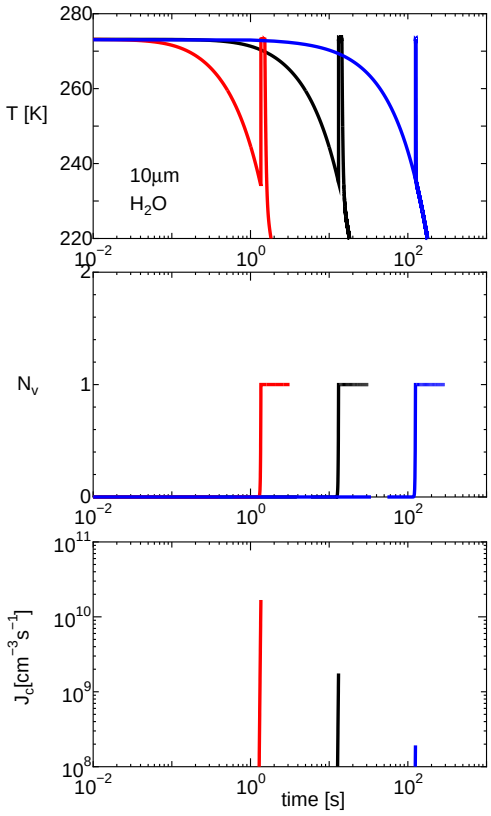

Fig. 4 Same as Fig. 3 but for various cooling rates (30 Ks^{-1} (red), 3 Ks^{-1} (black), and 0.3 Ks^{-1} (blue)). The crystallization temperatures are 234, 235, and 236 K for cooling rates of 30 Ks^{-1}, 3 Ks^{-1}, and 0.3 Ks^{-1}, respectively. In all cases, the particle contains unity number of nuclei.

stated in Section 1, the crystallization temperatures obtained in experiments are around 235 K, which minimally change over a wide range of cooling rates. Our analysis results are consistent with the experimental findings.

Fig. 5 shows the same evolutions as Fig. 3, but for various and larger cooling rates. The droplet size is 10 μm. The droplet crystallizes at cooling rates of 2.18×10^6 Ks^{-1} and 1.07×10^7 Ks^{-1}. Note that the number of critical nuclei is much larger than at the smaller cooling rates shown in Fig. 4, being 1.03×10^4 and 2.18×10^6 at cooling rates of 2.18×10^6 Ks^{-1} and 1.07×10^7 Ks^{-1}, respectively. In the case that the number of nuclei is larger than unity, polycrystal forms. The average size of polycrystal is given by $(V_0/N_v)^{1/3}$. Accordingly the average size of polycrystal is 0.46 μm (or 0.1 μm) for the cooling rate of 2.18×10^6 Ks^{-1} (or

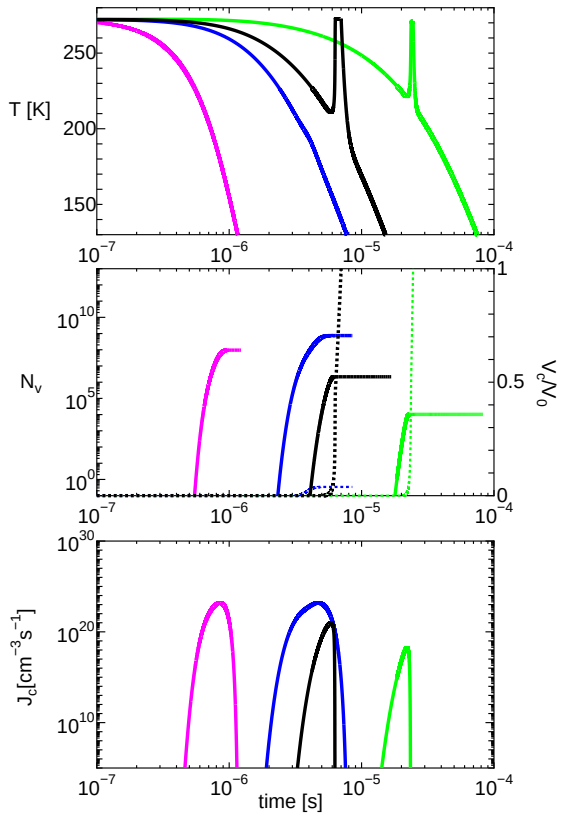

Fig. 5 Same as Fig. 3 but for various larger cooling rates. At cooling rates of 2.18×10^6 Ks^{-1} (green) and 1.07×10^7 Ks^{-1} (black), the crystallization temperatures are 221 K and 211 K, respectively, the numbers of critical nuclei are 1.03×10^4 Ks^{-1} and 2.16×10^6 Ks^{-1}, respectively, and the numbers of molecule included in a critical nucleus are 36 and 16, respectively. At much larger cooling rates (blue and pink curves correspond to the cooling rates of 2×10^7 Ks^{-1} and 1.3×10^8 Ks^{-1}, respectively), the crystallization hardly proceeds.

1.07×10^7 Ks^{-1}) in Fig. 5.

In the case of small cooling rates as shown in Fig. 4, once one nucleus forms, the nucleus grows fast due to high self-diffusivity and the crystallization proceeds quickly. This indicates that the first nucleus controls the droplet crystallization, i.e., there is less chance to form second nucleus. On the other hand, in the case of large cooling rates, a lot of nuclei forms because of large nucleation rate and crystal growth rate is small due to low temperature, indicating that the crystal growth rate controls the droplet crystallization rather than the nucleation. In Fig. 5, when the cooling rate exceeds 2.18×10^6 Ks^{-1}, the crystallization is incomplete because the self-diffusivity is too small (i.e., the viscosity is too high) to grow the crystal nuclei, although many nuclei form.

Figure 6 shows the same evolution as Fig. 3 but for various droplet sizes. The cooling rate is fixed at 30 Ks^{-1}. The crystallization temperatures depends on the droplet size, i.e., T_c =242, 235, and 223 K for 1000 μm, 10 μm, and 10 nm particles, respectively. This difference among the crystallization temperature can be explained by the waiting time before the nuclei form, which depends on the droplet volume. Accordingly, the crystallization starts earlier for the larger droplets at the same cooling rate.

In the present model, the interfacial tension was used by a standard model (Eq.(13)). To check the effect of interfacial tension on the temporal evolution of temperature, we changed the interfacial tension by $\pm$10% of the standard value. The results are plotted in Fig. 7. At a smaller interfacial tension, the crystallization begins earlier at higher temperature than the standard value because decreasing the interfacial tension enhances the nucleation rate. As shown in Fig. 7, a 10% change of the interfacial tension largely affects the crystallization temperature; specifically, decreasing (increasing) interfacial tension by 10% increases (decreases) the crystallization temperature by 6 K (7 K). Accordingly, the interfacial tension given by Eq.(13) can reasonably reproduce the crystallization temperatures obtained in the previous experiments.

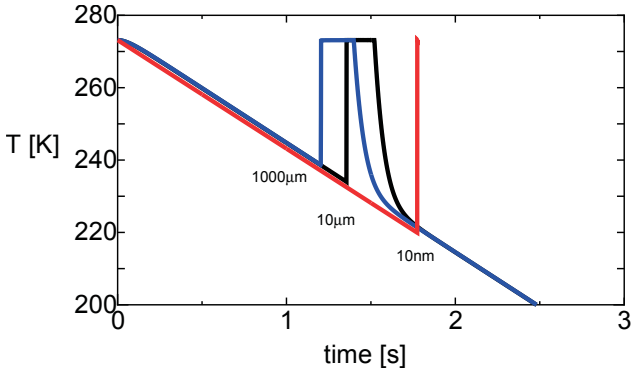

Fig. 6 Same as Fig. 3(a) but for various droplet sizes. The cooling rate is fixed at 30 Ks^{-1}. The crystallization temperatures of 1000μm, 10μm, and 10nm particles are 242, 235, and 223 K for respectively.

We then calculated the crystallization temperatures while varying the cooling rates and droplet size in the model (Fig. 8 and Table 3). The solid and dotted curves in Fig. 8 plot the crystallization temperatures as functions of cooling rate for 10 nm, 10 μm, and 1000 μm in the ASW and SCL diffusivity cases, respectively. The crystallization temperature is approximately given by $J(T_c)V_0\tau \simeq 1$ with a cooling time ($\tau = |T_m/(dT_{gas}/dt)|$). Table 3 displays the crystallization temperature, number of critical nuclei in the droplet, and the number of molecules included in the critical nucleus in each scenario.

As shown in Figure 8, the crystallization temperature of particles sized 1 μm to 1000 μm ranges from 230 K to 240 K at cooling rates below 10^4 Ks^{-1}. When the cooling rate exceeds 10^4 Ks^{-1}, the crystallization temperature decreases rapidly. On the other hand, the crystallization temperature of 10-nm particles is 200-230 K at cooling rates below 10^4 Ks^{-1}. When the droplets are small, the calculated crystallization temperature is larger in the ASW-diffusivity scenario than in the SCL-diffusivity scenario. This result suggests that the diffusivity of the supercooled liquid droplet better explains the experimental result of nano-sized droplets than the ASW diffusivity.

The maximum cooling rates calculated using the model (solid lines in Fig. 8) correspond to the critical cooling rates of vitrification. For the 10 nm, 10 μm, and 1000 μm sized particles, the vitrification rates are 2.9×10^6 Ks^{-1}, 8.9×10^6 Ks^{-1}, and 1.4×10^7 Ks^{-1}, respectively in the ASW-diffusivity scenario and 9.6×10^7 Ks^{-1}, 1.8×10^8 Ks^{-1}, and 1.8×10^8 Ks^{-1}, re-

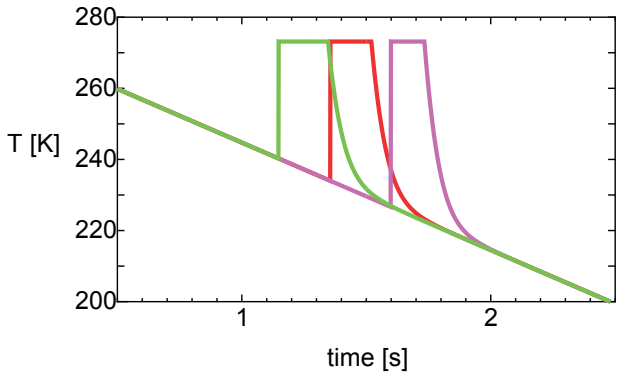

Fig. 7 Temperature evolution in the droplet particles with various interfacial tensions between the liquid and solid (0.9σ (green), σ, (red) and 1.1σ (purple)), where σ is given by Eq.(13). The droplet size is 10 μm and the cooling rate is fixed at 30 Ks^{-1}.

spectively, in the SCL-diffusivity scenario. Water droplets vitrify at an extremely large cooling rate (considered to exceed $\gtrsim 10^{6-7}$ Ks^{-1} [2,14,15]). The obtained critical cooling rates for vitrification are consistent with these of previous experiments.

In the present study, we considered both the ASW and SCL diffusivity constants. The results of two diffusivity scenarios are identical for large particle (1 μm to 1000 μm) because there is a negligible difference between two diffusivities at temperature around 235K (see Fig. 2). However, for small particles (10 nm), the crystallization temperature decreases, and the two diffusivity constants give largely different results, with the SCL diffusivity more accurately describing the experimental results than the ASW diffusivity. Experiments on small droplets provide low-temperature information (the no man's land region of the temperature versus cooling rate plot). Further experiments on particles sized 10-100 nm are necessary for a more detailed comparison.

As stated in Introduction, since water readily supercools, water clouds as well as fogs are frequently found in the atmosphere at temperatures below 0°C. The supercooled droplets have been observed at temperatures as low as -40°C all over the world (e.g., -35°C over Germany, -36°C over Russia, and -40°C over the Rocky Mts.) [32]. Cloud droplet sizes vary from a few micrometers to 50 μm with average diameters usually in the l0 to 20 μm range [33]. Since the cooling rates are considered to be in the range of 10^{-3} to 1 K s^{-1} [32,33], the crystallization temperatures evaluated by our analysis are 36-38°C, which are consistent with the observations. Our analysis is applicable in microphysics of clouds, especially the frozen probability in clouds.

4 Conclusions

We proposed a theoretical model that simultaneously describes nucleation and crystal growth in a water droplet. The model extends our previous model by incorporating the droplet size-dependence of the crystallization process. Especially, smaller droplets begin crystallizing later than larger droplets because they are less likely to form a nucleating center in a given time. For a given volume and cooling rate, this model computes the crystallization temperature and the number of crystal nuclei in the volume.

According to our model, the crystallization temperature depends on the droplet size and the cooling rate. The model well replicated the results of previous laboratory experiments, especially, the different responses of the crystallization temperatures of the micrometer- and nanometer-sized particles as function of cooling rates. For cooling rates below 10^4 Ks^{-1}, the crystallization temperature of particles sized 1 μm to 1000 μm was 230-240 K. For cooling rates beyond 10^4 Ks^{-1}, the crystallization temperature decreased rapidly. However, the crystallization temperature of the 10 nm particles was 200-230 K at the cooling rate below 10^4 Ks^{-1}. We also try two diffusion constants: the diffusivity of amorphous ice (ASW) and the diffusivity of supercooled liquid (SCL) water. At low cooling rates, the ASW and SCL diffusivities gave the same results for micrometer-sized particles, because these particles crystallize at temperature around the homogeneous nucleation temperature (235K), where both diffusivities are identical. However, for nanometer-sized particles, the crystallization temperature is lower and the SCL diffusivity is more accurate than the ASW diffusivity.

This model also elucidated the behavior of vitrifying water droplets. In the previous experiments, the critical cooling rate for vitrification was believed to exceed 10^{6-7} Ks^{-1}. In the SCL-diffusivity scenario, the critical cooling rates for vitrification were $\simeq 10^{7-8}$ Ks^{-1}, consistent with those of previous experiments.

The present analysis is useful not only for the comprehensively understanding the ice nucleation of droplets but also for application in various environments such as cirrus clouds. It will also supplement practical work by providing accurate predictions in difficult experimental scenarios.

Conflicts of interest

There are no conflicts to declare.

Acknowledgements

This work was supported in part by JSPS KAKENHI Grants No. 15H05731 and No. 18K03689.

Notes and references

1 A. Heymsfield and R. M. Sabin, *J. Atmos. Sci.*, 1989, **46**, 2252-2264.

2 P. G. Debenedetti, *Metastable liquids*, Princeton university press, 1996.

3 D. E. Hagen, R. J. Anderson and J. L. Kassner, Jr., *J. Atmos. Sci.*, 1981, **38**, 1236-1243.

4 D. Huang and L. S. Bartell, *J. Phys. Chem.*, 1995, **99**, 3924-3931.

5 B. Krämer, O. Hübber, H. Vortisch, L. Wöste and T. Leisner, *J. Chem. Phys.*, 1999, **111**, 6521-6527.

6 D. Duft and T. Leisner, *Atmos. Chem. Phys.*, 2004, **4**, 1997-2000.

7 S. Benz, K. Megahed, O. Möhler, H. Saathoff, R. Wagner and U. Schurath, *J. Photochem. Photobio. A: Cheristry*, 2005, **176**, 208-217.

8 P. Stöckel, I. M. Weidinger, H. Baumgärtel and T. Leisner, *J. Phys. Chem. A*, 2005, **109**, 2540-2546.

Table 3 Summary of our model results in two diffusivity scenarios (ASW and SCL): radius of water droplets, cooling rate, crystallization temperature T_c [K], number of critical nuclei, and the number of molecules in a critical nucleus.

radius	cooling rate [Ks^{-1}]	T_c [K] (ASW)	T_c [K] (SCL)	N_v (ASW)	N_v (SCL)	i_*(ASW)	i_*(SCL)
1000μm	10^{-3}	241.1	241.2	1.0	1.0	239	240
	10^{-2}	240.6	240.7	1.0	1.0	225	226
	10^{-1}	240.1	240.1	1.0	1.0	211	213
	1	239.5	239.6	1.0	1.0	198	200
	10	239.0	239.0	1.0	1.0	187	188
	10^2	238.3	238.0	1.0	1.0	173	174
	10^3	237.4	237.6	3.2	2.3	158	160
	10^4	235.4	235.9	241	86	128	134
	10^5	231.0	232.0	4.39×10^5	1.08×10^5	83	91
	10^6	225.0	226.9	4.88×10^8	7.21×10^7	48	57
	10^7	211.7	218.8	1.62×10^{13}	5.04×10^{10}	17	29
100μm	10^{-3}	239.5	239.6	1.0	1.0	198	200
	10^{-2}	238.9	239.0	1.0	1.0	185	187
	10^{-1}	238.3	238.4	1.0	1.0	173	174
	1	237.6	237.7	1.0	1.0	161	162
	10	236.9	237.0	1.0	1.0	149	150
	10^2	236.1	236.2	1.0	1.0	137	139
	10^3	235.3	235.4	1.1	1.0	126	128
	10^4	234.3	234.5	2.4	1.86	114	117
	10^5	230.7	231.7	780	187	81	89
	10^6	224.3	226. 4	1.1×10^6	1.4×10^5	45	55
	10^7	211.7	218.8	1.6×10^9	5.0×10^8	17	29
10μm	10^{-3}	237.6	237.7	1.0	1.0	161	163
	10^{-2}	236.9	237.0	1.0	1.0	149	151
	10^{-1}	236.1	236.2	1.0	1.0	137	139
	1	235.3	235.4	1.0	1.0	126	128
	10	234.4	234.6	1.0	1.0	115	117
	10^2	233.4	233.6	1.0	1.0	105	107
	10^3	232.4	232.6	1.0	1.0	95	97
	10^4	231.3	231.5	1.0	1.0	95	87
	10^5	229.6	230.1	1.0	3	73	76
	10^6	222.2	225.0	9148	880	38	48
	10^7	203.4	217.5	2.7×10^7	1.3×10^5	9.5	26
1μm	10^{-3}	235.3	235.4	1.0	1.0	126	128
	10^{-2}	234.4	234.6	1.0	1.0	115	117
	10^{-1}	233.4	233.6	1.0	1.0	105	107
	1	232.4	232.6	1.0	1.0	95	97
	10	231.3	231.5	1.0	1.0	85	87
	10^2	230.0	230.3	1.0	1.0	76	78
	10^3	228.7	229.0	1.0	1.0	67	69
	10^4	227.1	227.6	1.0	1.0	58	60
	10^5	225.4	225.9	1.3	1.1	50	52
	10^6	219.7*	222.8	40.5	6.9	31	40
	10^7	182.9*	214.3	4.5×10^5	880	2	20
10nm	10^{-3}	228.7	229.0	1.0	1.0	67	69
	10^{-2}	227.1	227.6	1.0	1.0	58	61
	10^{-1}	225.4	225.9	1.0	1.0	50	52
	1	223.4	224.1	1.0	1.0	42	45
	10	221.1	222.0	1.0	1.0	35	37
	10^2	218.4	219.5	1.0	1.0	28	31
	10^3	215.0	216.6	1.0	1.0	21	24
	10^4	211.0	213.3	1.0	1.0	16	19
	10^5	204.4	208.3	1.0	1.0	10	13.3
	10^6	195.1	202.4	1.0	1.0	5	8
	10^7	195.1	194.6	1.3	1.0	5	5

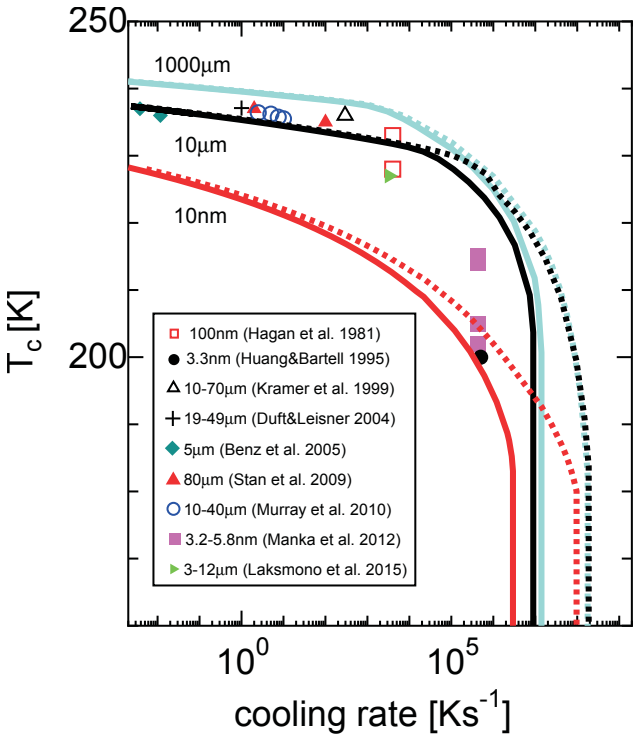

Fig. 8 The crystallization temperatures at various cooling rates obtained by our model in the ASW and SCL diffusivity scenarios (solid and dotted curves, respectively) and in the previous experiments of homogeneous ice nucleation (symbols). The particle size is varied as 10 nm, 10 μm, and 1000 μm. The critical cooling rates for vitrification are respectively 2.9×10^6 Ks^{-1}, 8.9×10^6 Ks^{-1}, and 1.4×10^7 Ks^{-1}, for 10 nm, 10 μm, and 1000 μm in the ASW diffusivity, and 9.6×10^7 Ks^{-1}, 1.8×10^8 Ks^{-1}, and 1.8×10^8 Ks^{-1}, for 10 nm, 10 μm, and 1000 μm in the SCL diffusivity.

9 C. A. Stan, G. F. Schneider, S. S. Shevkoplyas, M. Hashimoto, M. Ibanescu, B. J. Wiley and G. M. Whitesides, *Lab Chip,*, 2009, **9**, 2293-2305.

10 B. J. Murray, S. L. Broadley, T. W. Wilson, S. J. Bull, R. H. Wills, H. K. Christenson, and E. J. Murray, *Phys. Chem. Chem. Phys.*, 2010,**12**, 10380-10387.

11 A. Manka, H. Pathak, S. Tanimura, J. Wölk, R. Strey and B. E. Wyslouzil, *Phys. Chem. Chem. Phys.*, 2012, **14**, 4505-4516.

12 H. Laksmono, T. A. McQueen, J. A. Sellberg, N. D. Loh, C. Huang, D. Schlesinger, R. G. Sierra, C. Y. Hampton, D. Nordlund, M. Beye, A. V. Martin, A. Barty, M. M. Seibert, M. Messerschmidt, G. J. Williams, S. Boutet, K. Amann-Winkel, T. Loerting, L. G. M. Pettersson, M. J. Bogan and A. Nilsson, *Phys. Chem. Lett.*, 2015, **6**, 2826-2832.

13 T. Koop and B. J. Murray, *J. Chem. Phys.*, 2016, **145**, 211915(1-11).

14 P. Brüggeller and E. Mayer, *Nature*, 1980, **288**, 569-571.

15 E. Mayer and P. Brüggeller, *Nature*, 1982, **298**, 715-718.

16 L. Ickes, A. Welti, C. Hoose and U. Lohmann, *Phys. Chem. Chem. Phys.*, 2015, **17**, 5514-5537.

17 J. R. Espinosa, C. Vega and E. Sanz *J. Phys. Chem. C* 2018, **122**, 22892-22896.

18 K. K. Tanaka, T. Yamamoto, K. Nagashima and K. Tsukamoto, *J. Crystal Growth*, 2008, **310**, 1281-1286.

19 S. M. A. Malek, G. P. Morrow and I. S-Voivod, *J. Chem. Phys.*, 2015, **142**, 124506(1-15).

20 V. G. Baidakov and A. O. Tipeev, *J. Chem. Phys.*, 2012, **136**, 074510(1-9).

21 N. Okui, *J. Mat. Sci.*, 1990, **25**, 1623-1631.

22 A. Kouchi, T. Yamamoto, T. Kozasa, T. Kuroda and J. M. Greenberg, *Astron. Astrophys.*, 1994, **290**, 1009-1018.

23 S. C. Hardy, *Philos. Mag.*, 1977, **35**, 471-484.

24 L. Gránásy, T. Pusztai and P. F. James, *J. Chem. Phys.*, 2002, **117**, 6157-6168.

25 R. S. Smith and B. D. Kay, *Nature*, 1999, **398**, 788-791.

26 R. S. Smith, Z. Dohnálek, G. A. Kimmel, K. P. Stevenson and B. D. Kay, *Chem. Phys.* 2000, **258**, 291-305.

27 W. S. Price, H. Ide and Y. Arata, *J. Phys. Chem. A* 1999, **103**, 448-450.

28 S. Tachibana, A. Kouchi, T. Hama, Y. Oba, L. Piani, I. Sugawara, Y. Endo, H. Hidaka, Y. Kimura, K. Murata, H. Yurimoto and N. Watanabe, *Sci. Adv.*, 2017, **3**, eaao2538(1-6).

29 J. Wölk and R. Strey, *J. Phys. Chem. B* , 2001, **105**, 11683-11701.

30 D. M. Murphy and T. Koop, *Q. J. R. Meteorol. Soc.*, 2005, **131**, 1539-1565.

31 K. K. Tanaka, J. Diemand, H. Tanaka and R. Angelil, *Phys. Rev. E*, 2017, **96**, 022804(1-9).

32 H. R. Pruppacher and J. D. Klett, *Microphysics of Clouds and Precipitation*, Kluwer Academic Publishers, 1997.

33 J. H. Seinfeld and S. N. Pandis, *Atmospheric Chemistry and Physics*, John Wiley & Sons, INC. 1998.